

## **Supplementary Materials**

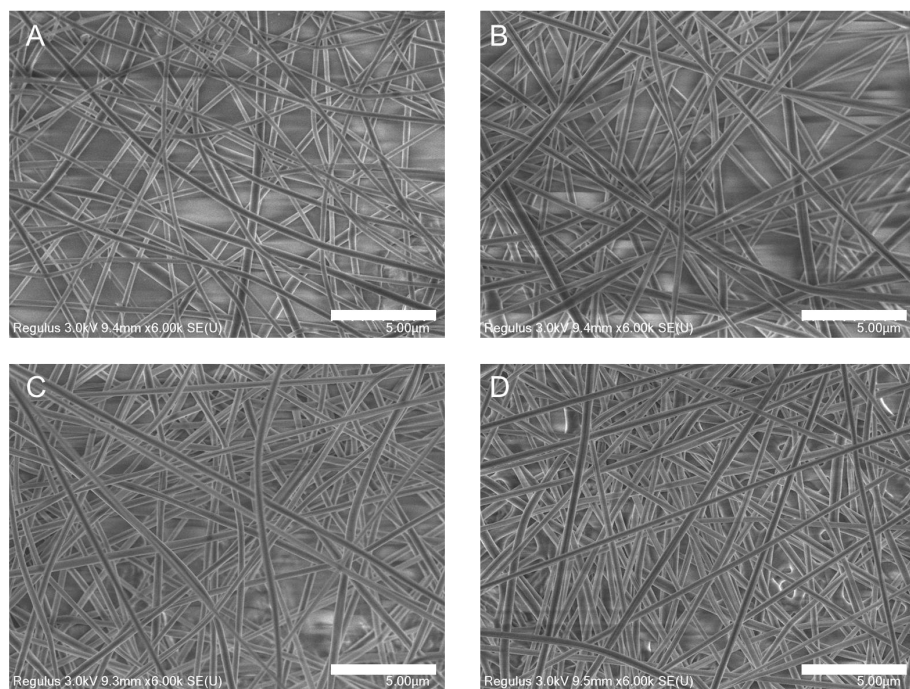
### **Air-gap-free epidermal bioelectronics via ethanol-triggered interfacial reconstruction for high-quality electrophysiological monitoring**

**Huijun Kong<sup>1</sup>, Chenshu Wu<sup>1</sup>, Cuiyu Liu<sup>1</sup>, Weiyan Li<sup>1</sup>, Li Niu<sup>2,\*</sup>, Zhongqian Song<sup>1,\*</sup>**

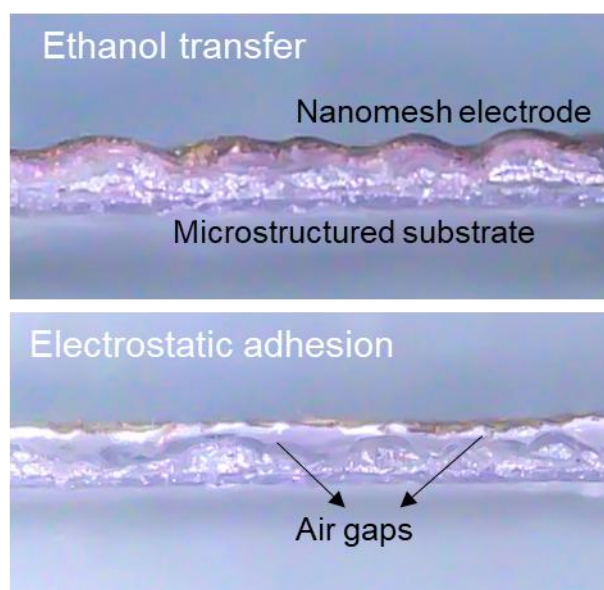
<sup>1</sup>School of Chemistry and Pharmaceutical Engineering, c/o College of Medical Information and Artificial Intelligence, Shandong First Medical University & Shandong Academy of Medical Sciences, Jinan 250117, Shandong, China.

<sup>2</sup>School of Chemical Engineering and Technology, Sun Yat-sen University, Zhuhai 519082, Guangdong, China.

**\*Correspondence to:** Prof. Zhongqian Song, School of Chemistry and Pharmaceutical Engineering, c/o College of Medical Information and Artificial Intelligence, Shandong First Medical University & Shandong Academy of Medical Sciences, Jinan 250117, Shandong, China. E-mail: zqsong@sdfmu.edu.cn; Prof. Li Niu, School of Chemical Engineering and Technology, Sun Yat-sen University, Zhuhai 519082, Guangdong, China. E-mail: niuli@mail.sysu.edu.cn

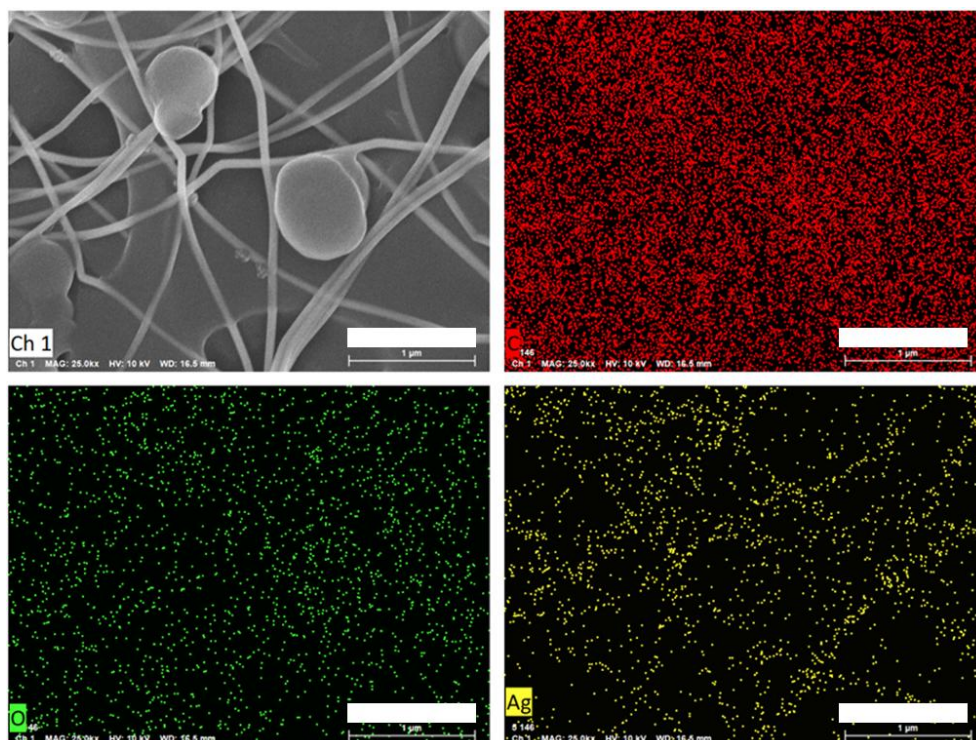


**Supplementary Figure 1.** SEM images of PVB nanofiber with various electrospinning time of 5 min (A), 10 min (B), 30 min (C) and 90 min (D). Scale bar: 5  $\mu$ m.

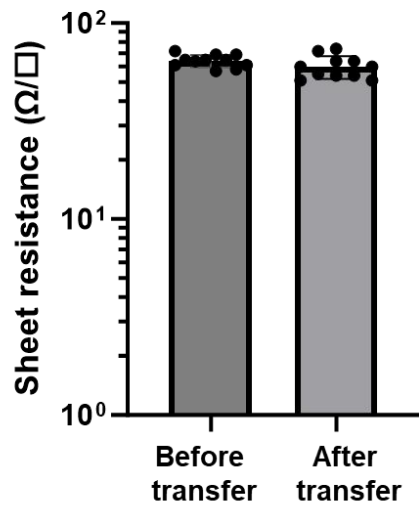


**Supplementary Figure 2.** Cross-sectional images of electrode-substrate interface with (top) and without (bottom) ethanol transfer process.

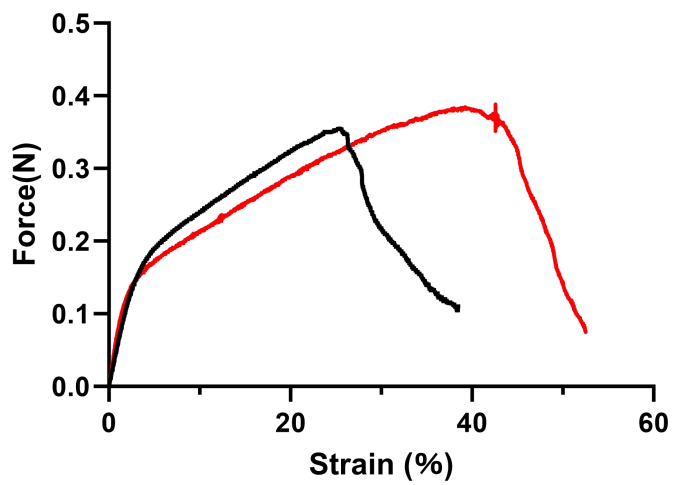
As shown in Supplementary Figure 2, the ethanol-assisted transfer enables intimate conformal contact between the nanomesh electrode and the microstructured substrate, with no observable interfacial air gaps. In contrast, the electrode attached via electrostatic adhesion exhibits clearly visible interfacial voids, provide direct structural evidence supporting the elimination of interfacial air gaps enabled by the ethanol-triggered interfacial reconstruction process.



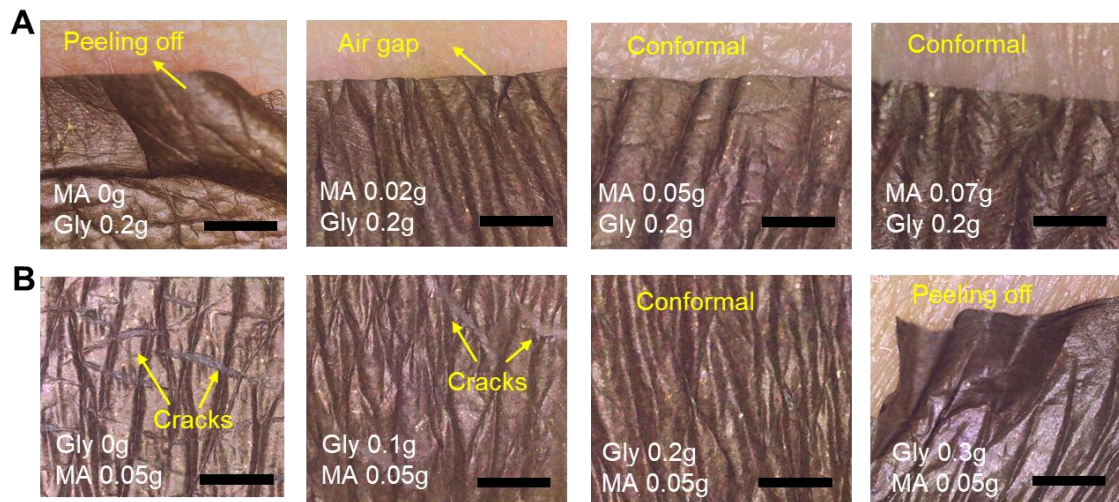
**Supplementary Figure 3.** Surface morphology of transferred nanomesh electrode and corresponding EDS mapping images of carbon (C), oxygen (O) and silver (Ag) elements. Scale bar: 1 $\mu$ m.



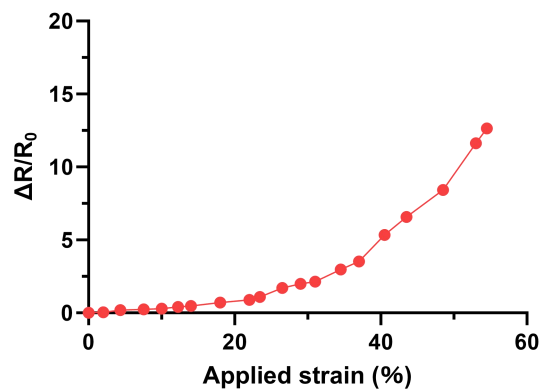
**Supplementary Figure 4.** The sheet resistance of the nanomesh electrode before and after transfer process.



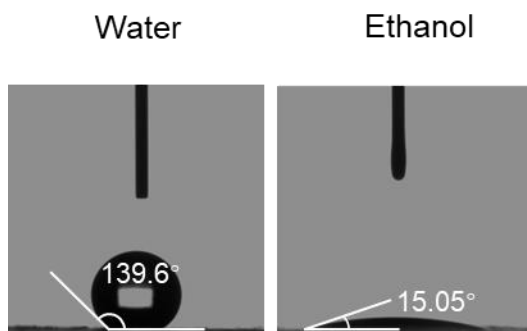
**Supplementary Figure 5.** Stress-strain curves of PVB nanomesh with and without glycerol.



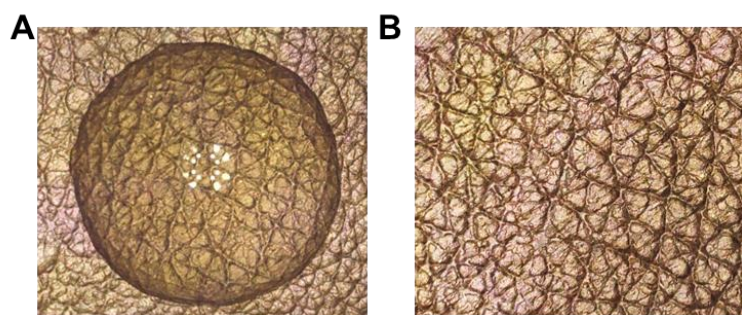
**Supplementary Figure 6.** (A) Photographs of nanomesh electrode attached on skin with various MA amounts after repeated skin deformation tests. (B) Photographs of nanomesh electrode attached on skin with various Gly amounts under skin stretching state.



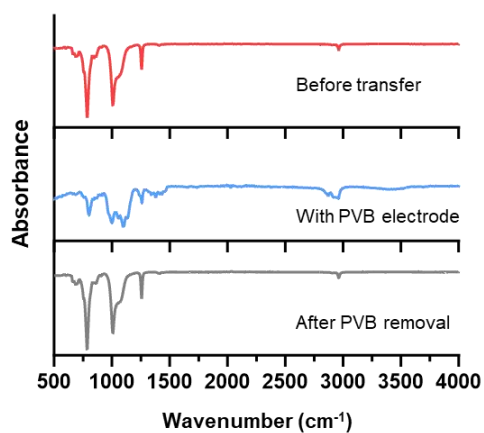
**Supplementary Figure 7.** The electrical resistance variation versus tensile strain for transferred nanomesh electrode.



**Supplementary Figure 8.** Contact angles of water (left) and ethanol (right) on the surface of nanomesh electrode.

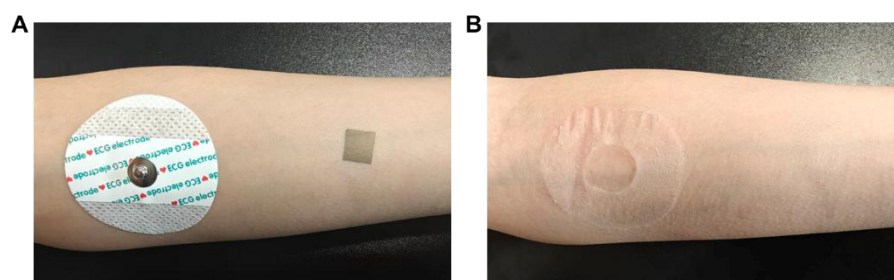


**Supplementary Figure 9.** Photographs of nanomesh electrode with a drop of water (A) and after removing the water drop (B).

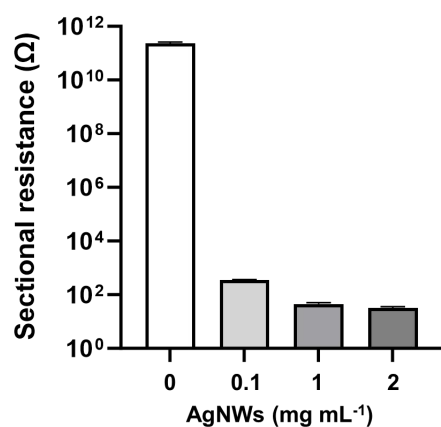


**Supplementary Figure 10.** FTIR spectrum of bare PDMS substrate, PDMS substrate with transferred PVB nanomesh, and after PVB removal.



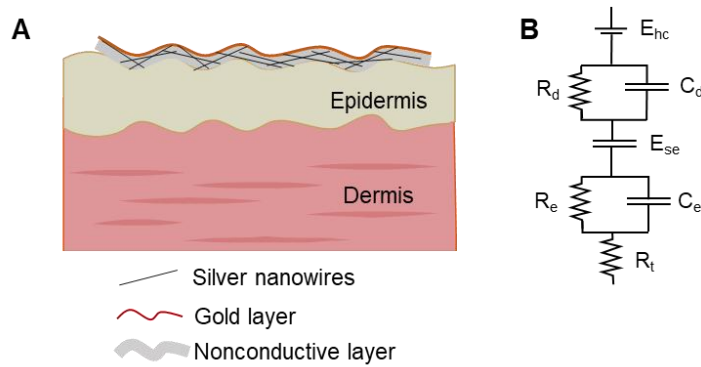


**Supplementary Figure 11.** (A) Photographs of the commercial gel electrode and nanomesh electrode attached onto human forearm, and corresponding images after 24-hour-skin attachment (B).



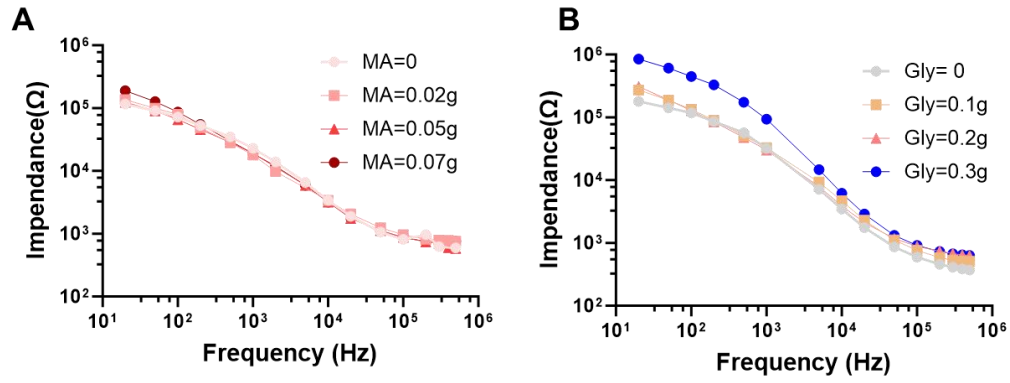
**Supplementary Figure 12.** The sectional resistance of nanomesh electrode with various AgNWs solutions (0, 0.1, 1 and 2 mg/ml) during transfer process.



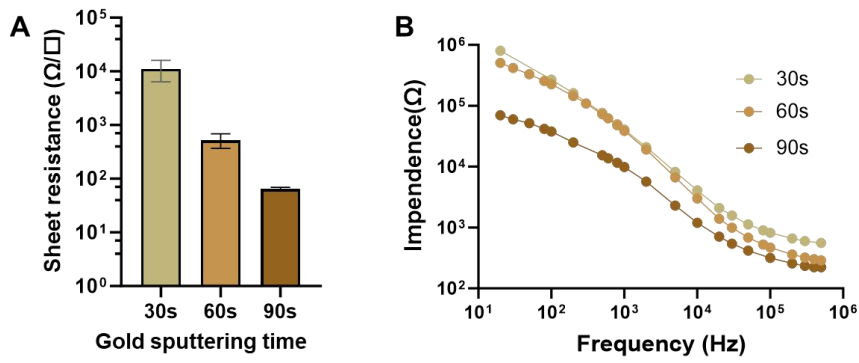


**Supplementary Figure 13.** The schematic illustration (A) and equivalent circuit (B) of the nanomesh electrode-skin interfacial system.

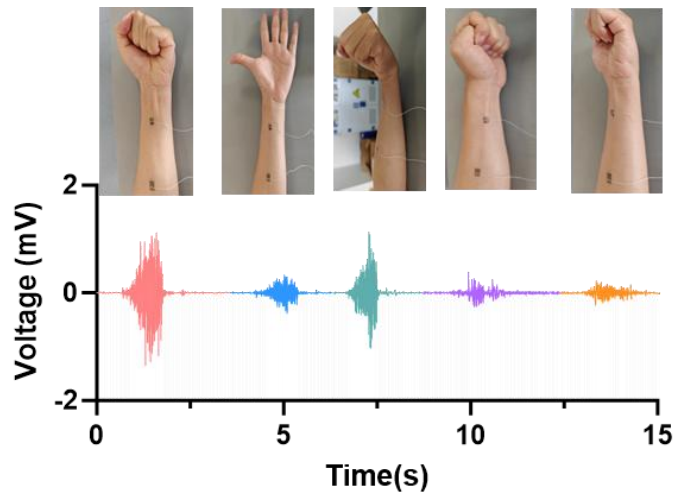
The acquisition of electrophysiological signals involves the transduction of ionic currents into electronic signals via epidermal electrodes. To clarify the charge transport mechanism, the equivalent circuit of the electrode-skin interface is illustrated in Supplementary Figure 13. In this model,  $R_t$  represents the resistance of the dermal layer, while the epidermis is modeled as a parallel combination of a resistor ( $R_e$ ) and a capacitor ( $C_e$ ), accounting for its resistive and capacitive characteristics.  $E_{se}$  denotes the potential arising from ion concentration differences across the stratum corneum. The electrode-skin interface is further described by a parallel circuit consisting of an interfacial capacitance ( $C_d$ ) and a charge transfer resistance ( $R_d$ ), where  $R_d$  denotes the resistance to ionic-electronic charge transfer across the interface. The embedded silver nanowire network provides continuous conductive pathways, facilitating efficient ionic-to-electronic signal transduction and thereby reducing the overall contact impedance of the electrode-skin interface.



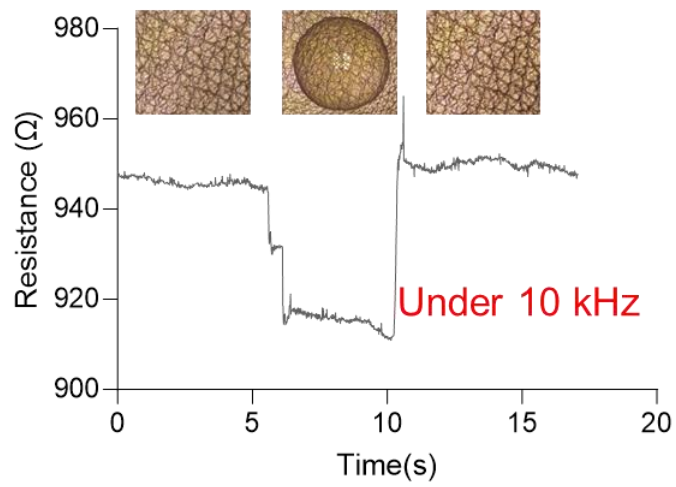
**Supplementary Figure 14.** The relationship between contact impedance and amounts of MA (A) and glycerol (B) in transfer solution.



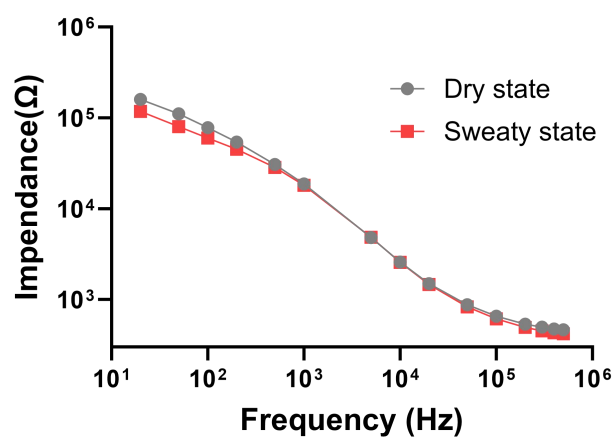
**Supplementary Figure 15.** (A) Sheet resistance of nanomesh electrode with various gold sputtering time of 30, 60, and 90s, and corresponding contact impedance after transferred onto human forearm (B).



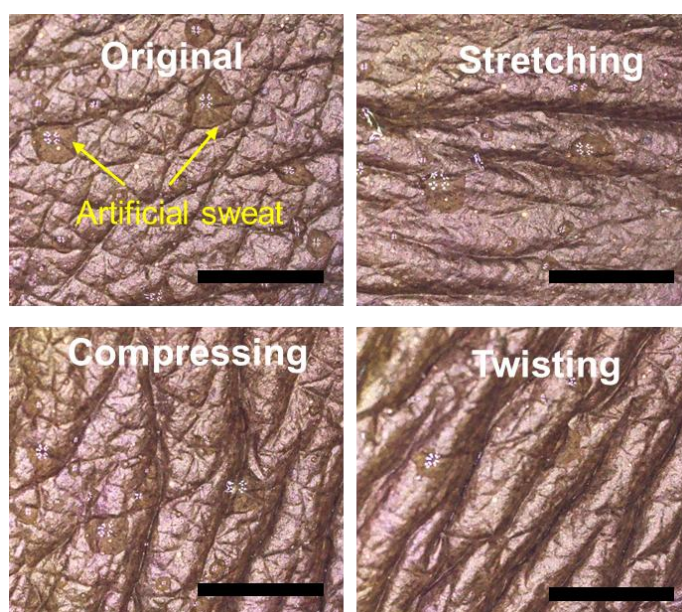
**Supplementary Figure 16.** The EMG signals acquired from nanomesh electrode with various muscle movements.



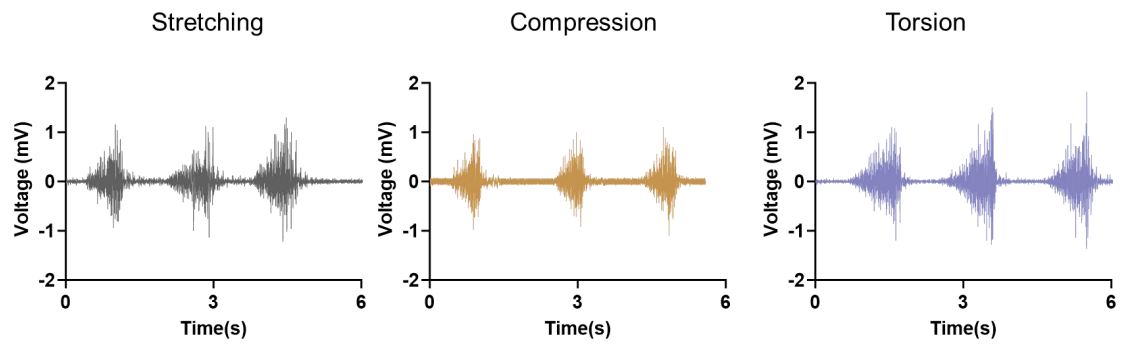
**Supplementary Figure 17.** Impedance of electrode-skin interface before and after positioned a drop of water.



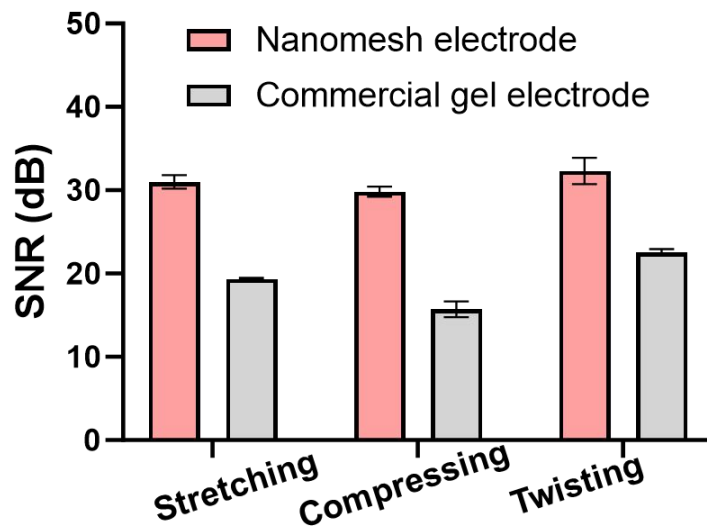
**Supplementary Figure 18.** Interfacial impedance of the nanomesh electrode measured under initial dry conditions and simulated sweaty state.



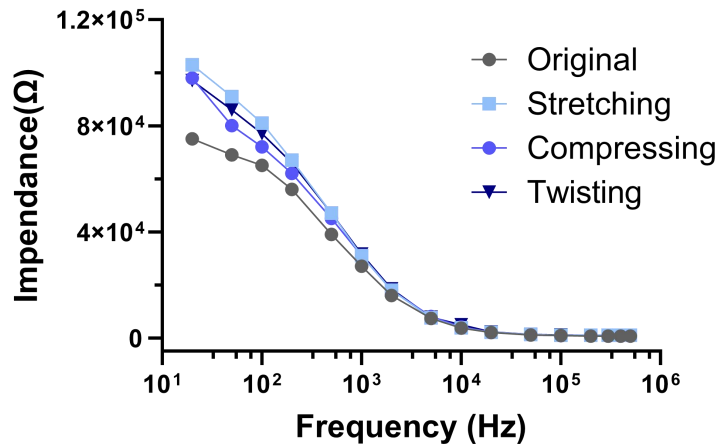
**Supplementary Figure 19.** The microscopic photographs of nanomesh electrode under simulated sweaty state with various skin deformations. Scale bar: 2 mm.



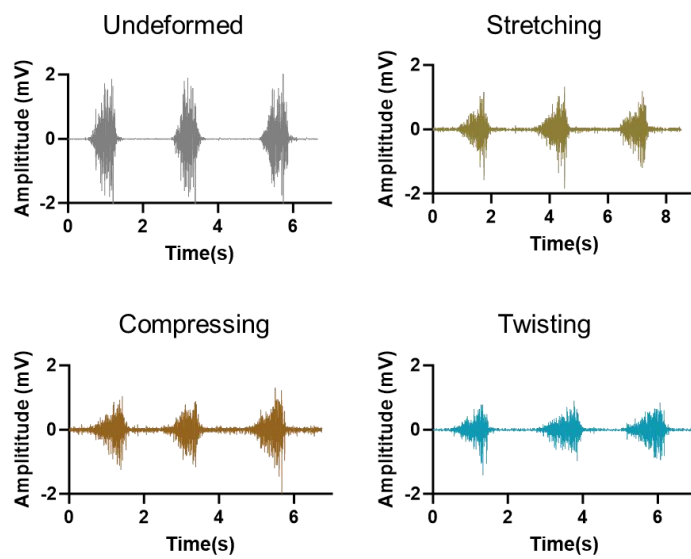
**Supplementary Figure 20.** EMG signals under skin stretching, compressing, and twisting states captured by commercial Ag/AgCl gel electrode.



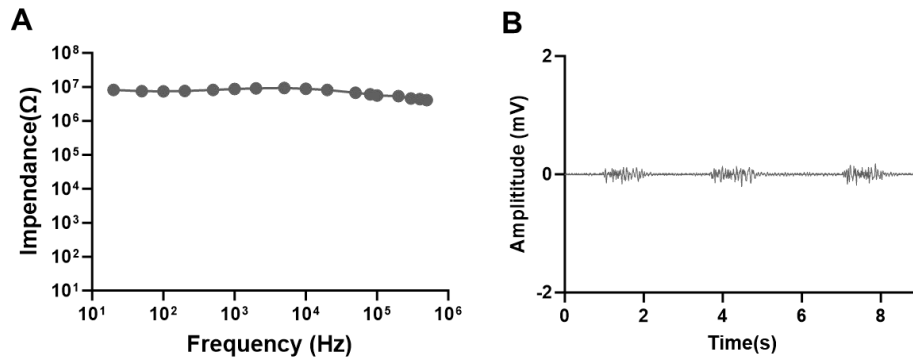
**Supplementary Figure 21.** SNR values of nanomesh electrode and commercial gel electrode under skin stretching, compressing and twisting conditions. The results are presented as mean  $\pm$  standard deviation,  $n=3$ .



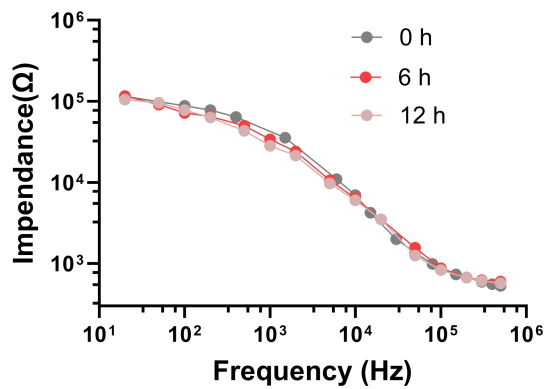
**Supplementary Figure 22.** Interfacial impedance transferred without medical adhesive under undeformed, stretching, compressing, and twisting deformation.



**Supplementary Figure 23.** EMG signals under skin deformations recorded by nanomesh electrode transferred without medical adhesive. The EMG signals exhibited severe signal attenuation under dynamic skin deformation, confirming the unstable interface transferred without medical adhesive.

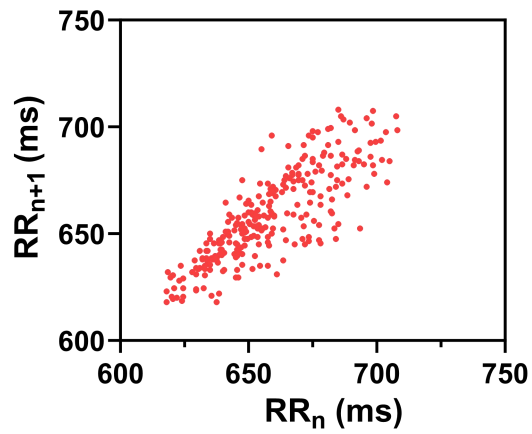


**Supplementary Figure 24.** Electrical performance of nanomesh electrode without transfer process, including frequency-dependent interfacial impedance (A) and the recorded EMG signals (B).

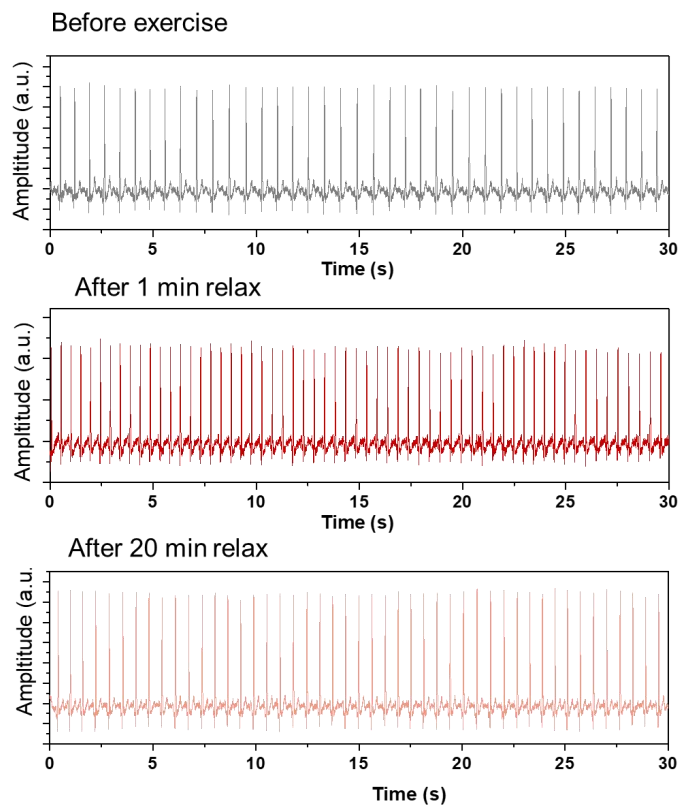


**Supplementary Figure 25.** Contact impedance of the nanomesh electrode-skin interface after skin attachment of 0 hour, 6 hours and 12 hours.

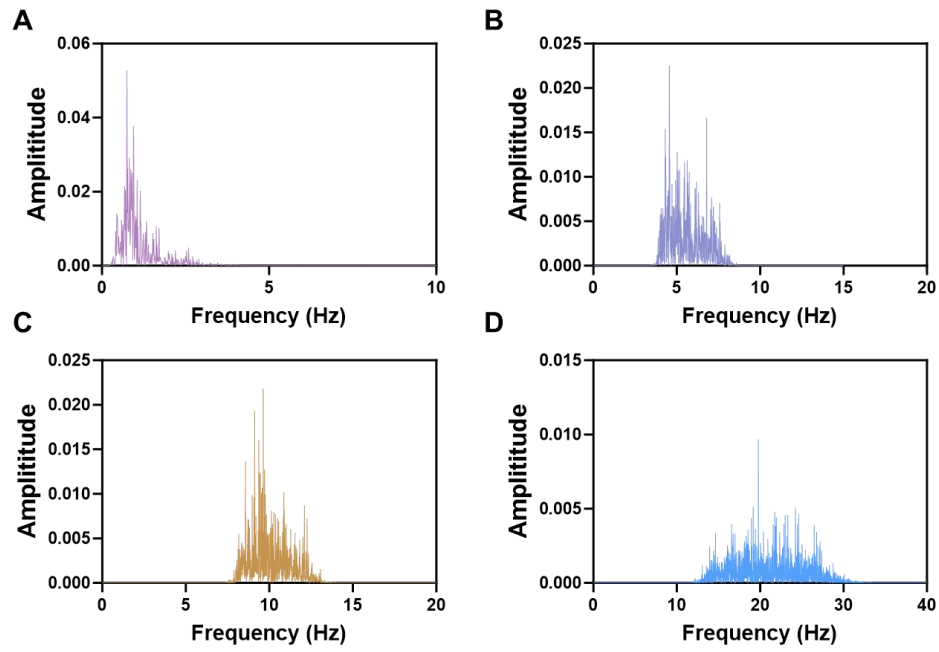




**Supplementary Figure 26.** Scatter plot distribution of R-R intervals in ECG signals collected by nanomesh electrodes.



**Supplementary Figure 27.** ECG signals captured by nanomesh electrodes before and after exercise (resting for one minute and twenty minutes).



**Supplementary Figure 28.** The extracted  $\delta$  wave of 0.5-4 Hz (A),  $\theta$  wave of 4-8 Hz (B),  $\alpha$  wave of 8-13 Hz (C) and  $\beta$  wave of 10-30 Hz (D) after fast Fourier transformation.

**Supplementary Table 1. Performance comparison between the nanomesh electrode and epidermal electrodes fabricated by other methods**

<b>Materials</b>	<b>Electrode type</b>	<b>Thickne ss</b>	<b>WVTR (g m<sup>-2</sup> h<sup>-1</sup>)</b>	<b>Contact impedance at 100 Hz (kΩ)</b>	<b>Water-conditi on measurement</b>	<b>Motion-artifa ct resistance</b>	<b>SNR</b>	<b>Ref</b>
Liquid metal	Dry electrode	8.3μm	53.4±1.15	360	Yes	Yes	34.5 EMG	[1]
PU/PVA hydrogel	Hydrogel electrode	5.3μm	77.3±1.53	21.0	N/A	Yes	19.0~20.1 EMG	[2]
LIG-assisted transfer of AgNWs network	Dry electrode	N/A	88.4	50	Yes	Yes	33.4 EMG	[3]
Electrospining hydroxypropyl methylcellulose	Dry electrode	18μm	102	~50	N/A	Yes	Over 20 EMG	[4]
PU/PVA/Gly/NaCl hydrogel	Hydrogel electrode	7μm	N/A	1.2	N/A	N/A	N/A	[5]
HPAN/PU/AgNWs	Dry electrode	15 μm	72.8	100	Yes	Yes	26 EMG	[6]

SPBS/ carbon filler	Dry electrode	N/A	N/A	132±23	N/A	Yes	40 ECG	[7]
Au/PI/PU	Dry electrode	72μm	N/A	~100	N/A	N/A	30 EMG	[8]
Ti/Au/Silbione /PDMS	Dry electrode	80–100μm	10.7	100	Yes	N/A	24.68 EMG	[9]
<b>PVB/Au</b>	<b>Dry electrode</b>	<b>5μm</b>	<b>60</b>	<b>37.8</b>	<b>Yes</b>	<b>Yes</b>	<b>42 EMG</b>	<b>This work</b>

**Supplementary Table 2. The heart-rate variability (HRV) indices extracted from the ECG signals**

	<b>Mean RR interval (ms)</b>	<b>SD1</b>	<b>SD2</b>	<b>SD1/SD2</b>
<b>Before exercise</b>	765.3	16.58	38.05	0.436
<b>After 1 min relax</b>	502.5	3.88	20.2	0.191
<b>After 20 min relax</b>	637.0	9.52	22.2	0.427

## References

- [1].Yan, W.; Liu, Y.; Wang, Y.; Yi, J.; Yang, J.; Wang, Z.; Sun, Q.; Zhou, P.; Zheng, M.; Huo, J.; Wang, Y., Conformal, Substrate-Free Liquid Metal Electrode for Continuous Health Monitoring. *ACS Sensors* **2025**, *10* (5), 3450-3460.DOI: 10.1021/acssensors.4c03449
- [2].Ye, X.; Li, L.; Wang, Z.; Wang, Y.; Yang, J.; Zheng, M.; Wang, M.; Ji, Z.; Lin, S.; Zhang, Y.; Luo, J.; Yi, J.; Zhou, P.; Cao, X.; He, X.; Wang, Y., Temporary Tattoo-Inspired, Skin-Adaptable Epidermal Electrode from an Ultrathin PU–PVA Film. *ACS Sensors* **2025**, *10* (8), 6218-6230.DOI: 10.1021/acssensors.5c02018
- [3].Li, J.; Zhang, S.; Zhong, J.; Bao, B.; Guo, K.; Zhang, Y.; Yang, K.; Tong, Y.; Qiu, D.; Yang, H.; Cheng, H., Laser-Induced Graphene-Assisted Patterning and Transfer of Silver Nanowires for Ultra-Conformal Breathable Epidermal Electrodes in Long-Term Electrophysiological Monitoring. *Adv. Funct. Mater.* **2025**, *35* (31).DOI: 10.1002/adfm.202504481
- [4].Ma, C.; Hao, S.; Yu, W.; Liu, X.; Wang, Y.; Wang, Y.; Zhao, J.; Zhang, N.; Bai, Y.; Xu, F.; Yang, J., Compliant and breathable electrospun epidermal electrode towards artifact-free electrophysiological monitoring. *Chem. Eng. J.* **2024**, *490*, 151118.DOI: 10.1016/j.cej.2024.151118
- [5].Gao, Q.; Sun, F.; Li, Y.; Li, L.; Liu, M.; Wang, S.; Wang, Y.; Li, T.; Liu, L.; Feng, S.; Wang, X.; Agarwal, S.; Zhang, T., Biological Tissue-Inspired Ultrasoft, Ultrathin, and Mechanically Enhanced Microfiber Composite Hydrogel for Flexible Bioelectronics. *Nano-Micro Letters* **2023**, *15* (1).DOI: 10.1007/s40820-023-01096-4
- [6].Yang, X.; Wang, S.; Liu, M.; Li, L.; Zhao, Y.; Wang, Y.; Bai, Y.; Lu, Q.; Xiong, Z.; Feng, S.; Zhang, T., All-Nanofiber-Based Janus Epidermal Electrode with Directional Sweat Permeability for Artifact-Free Biopotential Monitoring. *Small* **2022**, *18* (12).DOI: 10.1002/sml.202106477
- [7].Tian, Q.; Zhao, H.; Wang, X.; Jiang, Y.; Zhu, M.; Yelemulati, H.; Xie, R.; Li, Q.; Su, R.; Cao, Z.; Jiang, N.; Huang, J.; Li, G.; Chen, S.; Chen, X.; Liu, Z., Hairy-Skin-Adaptive Viscoelastic Dry Electrodes for Long-Term Electrophysiological Monitoring. *Adv. Mater.* **2023**, *35* (30), 2211236.DOI: 10.1002/adma.202211236
- [8].Chen, L.; Liang, H.; Liu, P.; Shu, Z.; Wang, Q.; Dong, X.; Xie, J.;

Feng, B.; Duan, H., Phase-Change Stamp with Highly Switchable Adhesion and Stiffness for Damage-Free Multiscale Transfer Printing. *ACS Nano* **2024**, *18* (35), 23968-23978.DOI: 10.1021/acsnano.4c00564

[9].Park, J.; Jeong, J.; Kang, M.; Pritish, N.; Cho, Y.; Ha, J.; Yea, J.; Jang, K.-I.; Kim, H.; Hwang, J.; Kim, B.; Min, S.; Kim, H.; Kwon, S.; Pak, C. J.; Suh, H. P.; Hong, J. P.; Lee, S., Imperceptive and reusable dermal surface EMG for lower extremity neuro-prosthetic control and clinical assessment. *npj flex. electron.* **2023**, *7* (1).DOI: 10.1038/s41528-023-00282-z